Molecular Crystals and Liquid Crystals
Publication details, including instructions for authors and subscription information:
http://www.tandfonline.com/loi/gmcl20

Synthesis and Characterization of an Insoluble Ruthenium-Based Coordination Polymer Catalyst for Water Oxidation

M. Mahdi Najafpour [a]
[a] Dorna Institute of Science, Khozestan, Iran

Version of record first published: 01 Mar 2010

To cite this article: M. Mahdi Najafpour (2010): Synthesis and Characterization of an Insoluble Ruthenium-Based Coordination Polymer Catalyst for Water Oxidation, Molecular Crystals and Liquid Crystals, 517:1, 167-179

To link to this article: http://dx.doi.org/10.1080/15421400903483916

Mol. Cryst. Liq. Cryst., Vol. 517: pp. 167–179, 2010

ISSN: 1542-1406 print/1563-5287 online
DOI: 10.1080/15421400903483916

Taylor & Francis
Taylor & Francis Group

Synthesis and Characterization of an Insoluble Ruthenium-Based Coordination Polymer Catalyst for Water Oxidation

M. MAHDI NAJAFPOUR

Dorna Institute of Science, Khozestan, Iran

In this study a novel linear coordination polymer catalyst, catena-poly[aqua {2-[6-(1,8-Naphthyrid-2-yl)-2-pyridyl]-1,8-naphthyridine}ruthenium(II)-μ-(4,4′-bipyridine)]perchlorate, di-sodium perchlorate, tri-ethanol solvate, is synthesized and characterized. This novel polymer is characterized by spectroscopy and solid-state electrochemical methods. In the presence of $Ce(NH_4)_2(NO_3)_6$, the polymeric catalyst is found to react with water and to efficiently and continuously liberate molecular oxygen (O_2). In electrochemical experiments, this catalytic process is confirmed, the activation energy for this process is estimated, and the potential dependence of the catalytic process is revealed.

Keywords Oxygen evolution; photosystem II; ruthenium complex; water oxidation

Introduction

Water oxidation to evolve O_2 is an important chemical reaction in photosynthesis. Water splitting is catalyzed by a $CaMn_4O_x$ complex housed in a special protein environment that also controls proton movements and the access of water [1]. This functional unit of photosystem II is referred to as the oxygen-evolving complex (OEC). Photosystem II created the aerobic atmosphere on earth and may serve as a model to split water by sunlight, which is necessary for a sustainable hydrogen economy [2]. In past few years, there has been a tremendous surge in research on the synthesis of various manganese complexes aimed at simulating OEC of photosystem II [3]. Ruthenium-based catalysts also show promise for water oxidation. One such system is the blue dimer $[\{cis\text{-}Ru(bpy)_2(H_2O)\}_2O](ClO_4)_4$ (bpy = 2,2′-bipyridine) in which the two Ru fragments are linked by a μ-oxo [4]; however, oxidation states lower than III, III cause the cleavage of the oxo bridge [5]. Zong and Thummel have synthesised a new family of ruthenium complexes for water oxidation [6]. In this report a polymeric and highly water insoluble ruthenium complex of similar ligand structure compared to the Thummel complex is synthesized and studied. This high insoluble polymer can be used as a heterogeneous catalyst as regards to advantages of heterogeneous processes versus homogeneous [7]. This

Address correspondence to M. Mahdi Najafpour, Dorna Institute of Science, No. 83 Padadshahr, 14 St. Ahwaz, Khozestan, Iran. E-mail: mmnajafpour@yahoo.com

newly designed coordination polymer has been found to catalyze the oxidation of water to oxygen driven electrochemically and also driven in the presence of a chemical oxidant ($(NH_4)_2[Ce\ (NO_3)_6]$).

Experimental Section

Material

All reagents and materials used for synthesis were reagent grade and used without further purification. Chemical reagents such as NH_4F, $RuCl_3 \cdot 3 \cdot H_2O$, 2-amino-3-pyridinecarbaldehyde, phosphoric acid, and KOH were obtained from Aldrich and used without further purification. Buffer solutions were prepared by addition of KOH into 0.1 M phosphoric acid. All solutions were prepared using de-ionized and filtered water with a resistivity of not less than 18 MΩ cm.

Physical Measurements

Analyses for carbon, hydrogen, and nitrogen were performed using a Heraeus elemental analyzer CHN-O-Rapid (Elementar-Analysesysteme, GmbH, Germany). Analyses for the metal ions were conducted using a Varian AA-220 spectrophotometer. IR spectra of KBr or NaCl pellets of the ligands and the complexes were recorded on an ABB Bomem MB series spectrophotometer in the range of 400–4000 cm^{-1}. Thermal stability and thermal transitions of the copolymer and terpolymer were observed by thermogravimetric analysis using a Shimadzu TGA-50 from 25 to 650°C (10°C min^{-1}) and a Shimadzu DSC-50 from 25 to 200°C (10°C min^{-1}), under N_2 atmosphere (50 mL min^{-1}). Scanning electron microscopy (SEM) measurements were conducted using a JEOL JXA-840 system. Oxygen evolution studies were carried out with luminescent DO probe type oxygen electrode (HQ40d portable dissolved oxygen meter) connected to the sample chamber was maintained at 37.1°C with a circulating water bath. In a typical run, the instrument readout was calibrated against air-saturated distilled water kept stirred in the air-tight sample chamber under the Clark electrode. After ensuring a constant baseline reading, the water was taken out, and 10 mL of Ce(IV) was introduced into the sample chamber. After allowing time for equilibration (~1 min), the complex as a solid was injected into Ce(IV). In control experiments, 1 mL of blank solvent was added to 25 mL of the Ce(IV). The control readings were subtracted from the sample readings to get the final oxygen-evolution data. The subtraction of controls typically produced less than a 1% change in the oxygen-evolution data. The experimental setup consists of home-made jacketed glass cell with a threaded neck and a capillary side-arm for catalyst injection. The cell was charged with Ce(IV). Ceric ammonium nitrate (0.1 g, 0.15 mmol) dissolved in 10 ml water magnetically stirred at 37.1°C. Ce(IV) was stable in this condition and oxygen evolution was not observed. After de-aeration of Ce(IV) with nitrogen, the complexes (0.1 mg) as solid suspension were added, and oxygen evolution was recorded with the oxygen meter under stirring. The data were sent directly to a computer. Voltammetric experiments were performed with a micro-AutolabIII system (Eco Chemie, Netherlands) in a standard three terminal electrochemical cell with a saturated calomel reference electrode, SCE (Radiometer, Copenhagen) placed ca. 0.5 cm from the working electrode, and a 2 cm × 2 cm platinum gauze counter electrode. The working electrode was a basal

plane pyrolytic graphite electrode (4.9 mm diameter, Le Carbon, UK) mounted in Teflon. Prior to voltammetric experiments solutions were de-aerated with argon (BOC). The powder (ca. 1 mg) was placed on a filter paper (Whatman 1), and a basal plane pyrolytic graphite electrode was pressed and moved onto the powder. This caused a small amount of the powder sample to adhere to the graphite electrode surface. The electrode is then immersed in aqueous electrolyte solution and voltammetric data are recorded.

Synthetic Procedures

2-[6-(1,8-Naphthyridin-2-yl)-2-pyridyl]-1,8-naphthyridine (1). To a mixture of 2,6-diacetylpyridine (1.02 mmol) and 2-aminonicotinaldehyde (2.09 mmol) in absolute ethanol (20 mL) was added a solution of KOH (0.05 g) in absolute ethanol (5 mL). The mixture was refluxed for 12 h under Ar, and kept at room temperature overnight. A light yellow precipitate was collected and washed with absolute ethanol [8]. (Found: C, 75.1; H, 3.8; N, 21.0%. Calc. for $C_{21}H_{13}N_5$: C, 75.2, H, 3.9; N, 20.9%).

Catena-poly[aqua{2-[6-(1,8-Naphthyrid-2-yl)-2-pyridyl]-1,8-naphthyridine} ruthenium(II)-μ-(4,4′-bipyridine)] perchlorate (2). A suspension of 1 (167 mg, 0.5 mmol) in absolute ethanol (20 mL) and an ethanolic solution (10 mL) of $RuCl_3 \cdot 3H_2O$ (150 mg, 0.58 mmol) were mixed at room temperature, and the mixture was then refluxed for 1.5 h. To the mixture were added 4,4′-bpy (78 mg,

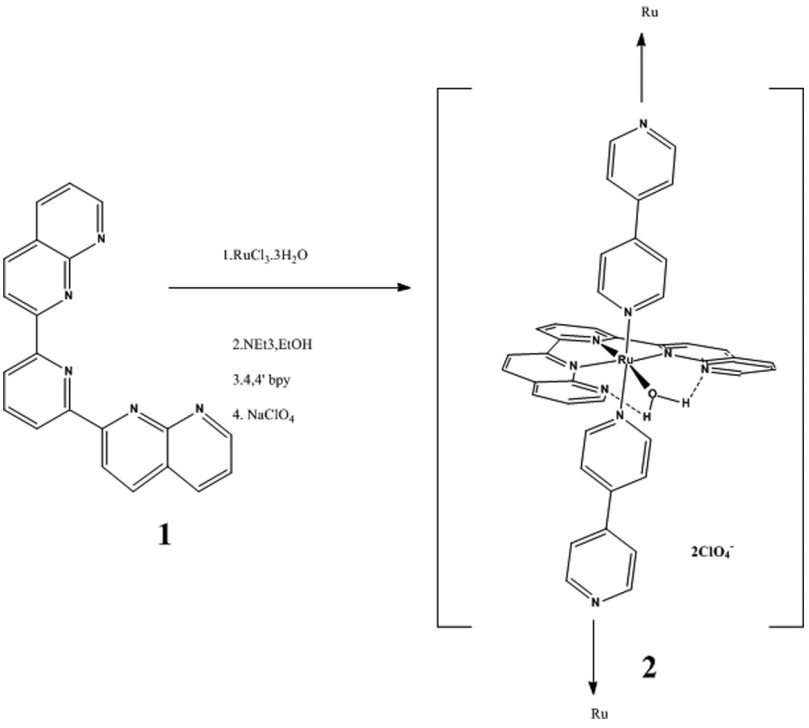

Scheme 1. Reaction pathway for the synthesis of the complex.

0.5 mmol), water (10 mL), and triethylamine (0.2 mL) and the mixture was further refluxed for 43 h. The solution was concentrated to about 10 mL, followed by the addition of aqueous $NaClO_4$. The precipitate was filtered and washed with water, ether, and acetone (Scheme 1). The polymeric nature of the complex make purification and characterization more complicated, but ultimately create a new type of catalyst. IR (KBr, cm^{-1}) 3444, 1602, 1415, 1085, 804. The elemental analysis is consistent with 2 (Found: C, 38.5; H, 3.4; N, 8.9%. Calc. for $2.2NaClO_4 \cdot 3EtOH$ ($C_{37}H_{39}Cl_4N_7Na_2O_{19}Ru$): C, 37.8, H, 3.4; N, 8.3%). The material is X-ray diffraction amorphous.

Results and Discussion

IR Spectrum

The IR spectra (Fig. 1) of the complex shows a broad band due to water centered at 3400 cm^{-1}. The appearance of band at 1090 and 620 cm^{-1} are indicative of the presence of perchlorate group [9]. Peaks revealing the presence of ligand in the complex occur in the ranges 3100–2900 cm^{-1} (aromatic C-H stretching vibrations), 1600–1550 cm^{-1} [ν (C=N) and ν (C=C) stretches], 1470–1020 cm^{-1} [ν(C-C) + ν (C-N) vibrations], and 810–710 cm^{-1} (aromatic C-H deformation vibrations).

Raman Spectrum

A tentative assignment of the vibrational observed in the resonance Raman spectra was by comparison with the related systems literature [10–12], as shown in Table 1.

Thermal Analysis

For the complex a loss of mass (3%) (EtOH) was found in the interval from 27 to 127°C. After reaching a temperature of 351°C mass loss takes place due to ligand decomposition, reaching a maximum at 643°C, where approximately 50% mass loss is observed (Fig. 2).

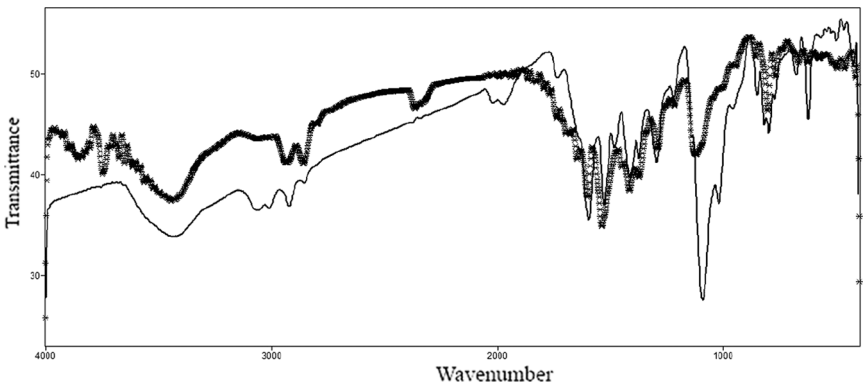

Figure 1. IR spectra of the polymeric complex after (points) and before (line) oxygen evolution experiments.

Table 1. Resonance Raman frequencies cm^{-1} for the complex

1600	ν (CC)
1400	ν (CC, CN)
1350	ν (CC, CN) + δ (CCH)
1320	ν (CC, CN) + δ (CCH)
1160	δ (CCH, CCC)
1120	δ (CCH)
1043	ν (CC, CN)
700	Δ (CCC in-plane)

SEM

SEM image of the complex is shown in Fig. 3. Any crystalline forms are not observed in the complex. SEM observation showed that it appeared to consist of agglomerates of the 0.2–0.4 μm particles.

Mass Spectral Analysis

A summary of the highest mass peaks from the FAB mass spectral analysis of the title complex is given in Table 2 and support information.

Oxygen Evolution

Although the thermodynamic, reversible cell voltage for water electrolysis is ≈1.2 V under moderate conditions (50–100°C, a few atmospheres of pressure), the anodic reaction is overwhelmingly rate limiting, resulting in substantial electrode overvoltages (≈1 V) when working at current densities required for practical operation [2]. This impacts directly on conversion efficienty. It is suggested [13,14] that hydrogen bond is very important in oxygen evolution and it could decrease activation

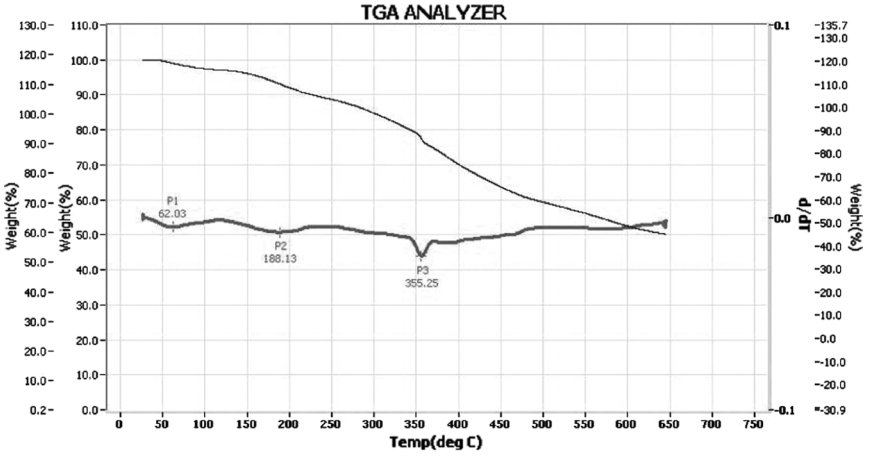

Figure 2. Thermoanalytical (TG and DTG) curves for the complex.

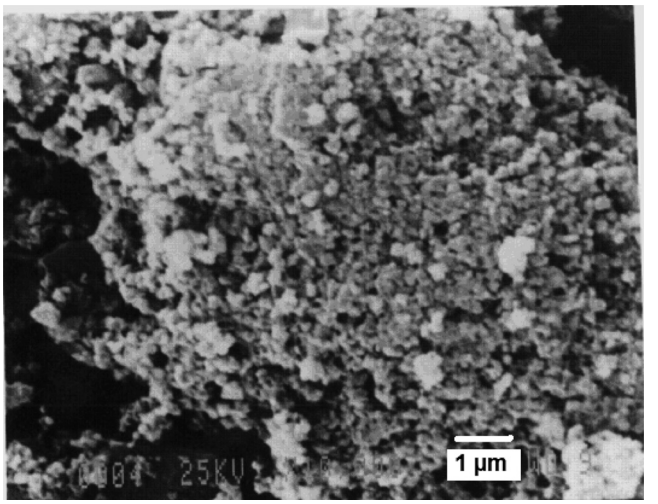

Figure 3. The SEM image of the complex (×10000).

energy for water oxidation; for example, this could result in a weakening of the M-OH (hydrogen bond increases positive charge of oxygen; this could result in a weakening of the M-OH and decreases activation energy). In this complex, the water molecule is H-bonded to an uncoordinated naphthyridine nitrogen on ligand. This hydrogen bond could be important in water oxidation. The cell was charged with $(NH_4)_2[Ce(NO_3)_6]$ (0.1 g, 0.15 mmol) dissolved in 10 ml water magnetically stirred at 37.1°. After the de-aeration (with nitrogen) complex (0.1 mg) as solid suspension was added, and O_2 evolution was recorded with an oxygen meter under stirring (Fig. 4). Control experiments with ligand (**1**) and $RuCl_3$ gave no oxygen. Control experiments with RuO_2 gave low oxygen as compared with the complex.

Total volume of oxygen is 0.9 ml (by volumetric analysis) which corresponds to ~90% of the total amount of Ce^{IV} added. After oxygen evolution experiment catalyst shows no change in IR spectrum (Fig. 1) and can be used again for water oxidation. To ensure that the formed oxygen originates from water rather than from the nitrate of ceric ammonium nitrate, cerium(IV) trifluoromethanesulfonate (OTf^-) was used as an oxidant. It was found that the use of $Ce(OTf)_4$ in place of ceric ammonium nitrate also leads to oxygen production, confirming that water is being

Table 2. MALDI mass spectral data for the complex

m/z	Rel. Abund.	Assignment
336	100	$[LH]^+$
436	8	$[RuL]^+$
454	5	$[RuL(H_2O)]^+$
692	2	$[RuL(H_2O)\ (4.4'\text{-bpy})ClO_4]$
766	1	$[RuL(H_2O)\ (4.4'\text{-bpy})_2]^+$

L: 2-[6-(1,8-Naphthyridin-2-yl)-2-pyridyl]-1,8-naphthyridine.

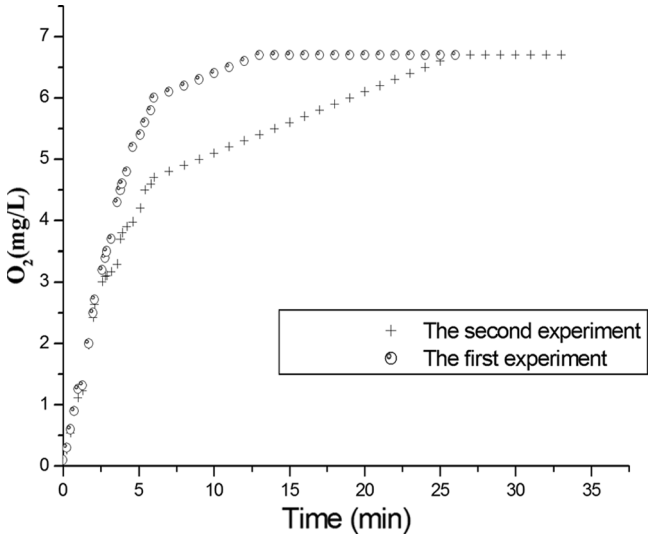

Figure 4. Time-dependence of O_2-evolution (0.1 g, 0.15 mmol) $(NH_4)_2[Ce(NO_3)_6]$ was dissolved in 10 ml water after the de-aeration (with nitrogen); 0.1 mg complex as solid suspension was added, and O_2 evolution was recorded with an oxygen meter under stirring ($T = 37.1°$). The complex can be used again after washing (small figure).

oxidized in these reactions. The nature of the catalytic surface species is currently not known, but it is likely that the coordination polymeric material remains intact during water splitting. The oxidation by the plymer ligand–metal complex catalyst is considered as a noteworthy reaction that a polymer catalyst had higher activity than a low molecular weight catalyst. The best TNs were from 260 (mononuclear) to 689 (dinuclear) for similar complexes as homogenous catalysts [6]. The polymer as a heterogeneous catalyst showed more TN (~2500). Another important aspect related to this polymer is its heterogenization, given the advantages of heterogeneous processes versus homogeneous. Those advantages include ease of catalyst separation, minimization of inter-catalyst deactivation.

Solid State Electrochemical Characterization of the Complex

Insoluble solid materials such as metal oxide or polymer powders are important components in electrochemical devices, and often the study of solids, e.g., for catalysis in electrochemical systems is important. The voltammetry of insoluble solid powder samples has been developed [15] to provide a general tool to study solid-state electrochemical reactivity for example of water-insoluble transition metal complexes [16]. Here, the polymeric and highly insoluble catalyst is studied in powder form to provide more insight into the effects of applied potential. The voltammetric characteristics of the insoluble metal complex were explored in aqueous media in order to demonstrate catalytic activity for oxygen evolution process. The solid was obtained in powder form and immobilized at the surface of a basal plane pyrolytic graphite electrode. The immobilization procedure was based on embedding the powder into the graphite surface by polishing on a filter paper (see Experimental). Stable modified electrodes were obtained.

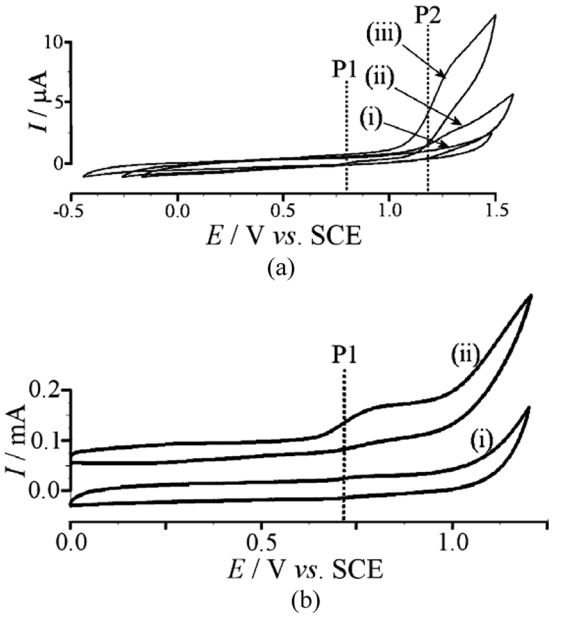

Figure 5. (a) Cyclic voltammograms (scan rate $0.1\,V\,s^{-1}$) obtained for (i) a bare basal plane pyrolytic graphite electrode, (ii) a complex modified basal plane pyrolytic graphite electrode at 20°C, and (iii) a complex modified basal plane pyrolytic graphite electrode at 40°C immersed in aqueous 0.1 M NH_4F solution. (b) Cyclic voltammograms (scan rate $0.1\,V\,s^{-1}$) obtained for a complex modified basal plane pyrolytic graphite electrode at (i) 20°C and (ii) 60°C immersed in aqueous 0.1 M phosphate buffer (pH 7) solution.

Initial experiments were performed in aqueous NH_4F as an electrolyte with low hydrophobicity and coordination ability. Figure 5 shows typical voltammograms obtained in aqueous 0.1 M NH_4F solution. A bare graphite electrode (see trace i) shows no signal. However, after embedding the complex material, a clear oxidation process (P2) is observed commencing at a potential of ca. 1.2 V vs. SCE. This process remained stable, and the catalyst active over many potential cycles and oxygen evolution is the most likely process to occur under these conditions. Oxygen evolution has no effect on electrochemical behavior. The oxygen evolution is also reproducibile. Even more dramatic are results at slightly elevated temperatures. A 20 degree increase in the solution temperature (compare curves ii and iii) causes the current to increase by a factor of approximately 5 for P2 (the activation energies of P1 and P2 are equal). This result may be interpreted in terms of an activation energy for the rate determining step of approximately $E_A = 60\,Kj\,mol^{-1}$ (see Eq. (1)):

$$\ln\left(\frac{I_{T_1}}{I_{T_2}}\right) = \frac{E_A}{R} \times \left(\frac{1}{T_2} - \frac{1}{T_1}\right). \tag{1}$$

In this equation, the currents I_{T_1} and I_{T_2} are assumed to represent the kinetically limited process of oxygen evolution. The result demonstrates that the complex is a powerful oxygen evolution catalyst with strong temperature dependence. It is interesting to explore the lower current range, and indeed at 40°C (curve iii), there

appears to be an additional signal with an onset potential of ca. 0.8 V vs. SCE (P1). This process suggests even more dramatic catalysis effects. The interpretation of processes P1 and P2 is possible by assuming a "surface-based" process (P1) and a "bulk-based" process (P2) [17]. The nature of these two processes may be very similar except that process P2 may requires a bulk exchange of electrons and ions which is not required for the redox process P1 at the particle surface.

In order to further study the effect of electrolyte and pH, a series of experiments in phosphate buffer electrolyte were undertaken. Figure 6 shows voltammograms for the oxidation of immobilized the complex obtained at 20°C, 40°C, and at 60°C. In all cases, the oxidation process P1 and at more positive potentials the process P2 can be identified. In phosphate buffer, the oxidation responses are observed over several potential cycles but show a slow decay in particular at slow potential scan rates. The temperature again has a considerable effect on the electrochemical process, and in particular at 60°C the oxidation is clearly observed. The position of the onset potential for process P1 is consistent with that observed in NH_4F (see Fig. 5). Next, the effect of the scan rate on the voltammetric signals was studied. Figure 6 shows voltammograms obtained at 40°C and recorded at $5\,mV\,s^{-1}$, $20\,mV\,s^{-1}$, and at $100\,mV\,s^{-1}$. At slower scan rate, the second oxidation process, P2, is more prominent and the peak for this process is shifted more positive as the scan rate increases. At the same time, the signal for the process P1 is significantly increased. The plot in Fig. 6d

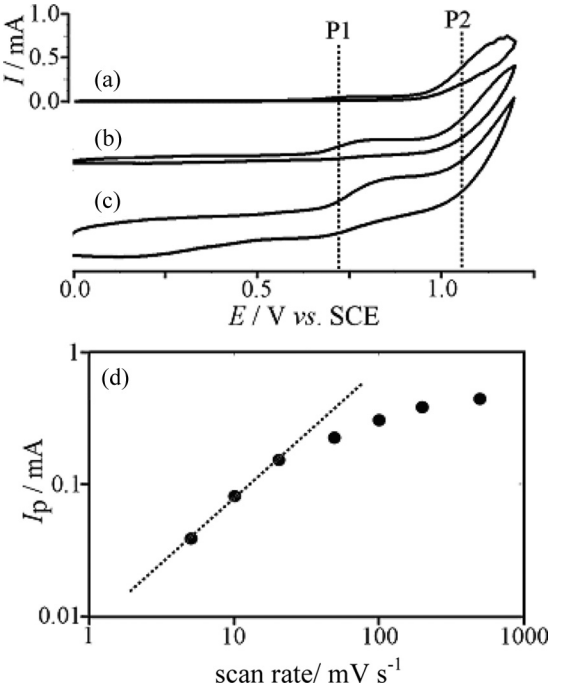

Figure 6. Cyclic voltammograms (scan rate (a) $0.005\,V\,s^{-1}$, (b) $0.02\,V\,s^{-1}$, (c) $0.1\,V\,s^{-1}$) obtained for a complex modified basal plane pyrolytic graphite electrode at 40°C immersed in aqueous 0.1 M phosphate buffer (pH 7) solution, and (d) Plot of the anodic peak current for process P1 vs. the scan rate. The dashed line is indicating the proportionality expected for thin immobilised films.

shows the approximate peak or limiting current plotted versus scan rate. The double logarithmic scale allows a linear relationship between current and scan rate to be observed only at very low scan rates. This behavior is characteristic for immobilized redox systems and not anticipated for a catalytic process. For electrocatalytic processes no dependence on scan rate is expected, and therefore the contribution of the electrocatalytic process to the current appears to be small. The presence of phosphate may inhibit the catalytic activity. At scan rate higher than 500 mV s^{-1}, the current associated with process P1 becomes ill-defined, and it seems to merge with the background current (not shown). At scan rates of 100 mV s^{-1} and higher, also cathodic peaks become noticeable which may indicate an intermediate Ru^{III} state which only slowly undergoes reaction with water (Scheme 2). A set of experiments were conducted at 40°C and in phosphate buffer solution systems with a range of pH values. The onset potential for process P1 was chosen as a pH sensitive parameter. Figure 7 shows voltammograms obtained at pH 5, 7, and 9, and although the oxidation peak is difficult to identify, a shift with pH is clearly observed. A plot of E_{onset} data points vs. pH is shown in Fig. 7d, and it reveals a shift approximately consistent with a Nernstian slope of 59 mV/pH unit. Although the measured E_{onset} value is unlikely to be thermodynamically defined, the correlation seems to suggest that proton release is coupled to the electron transfer process. It is possible that the oxidation of the complex redox center is linked to the release of a proton (e.g., from a

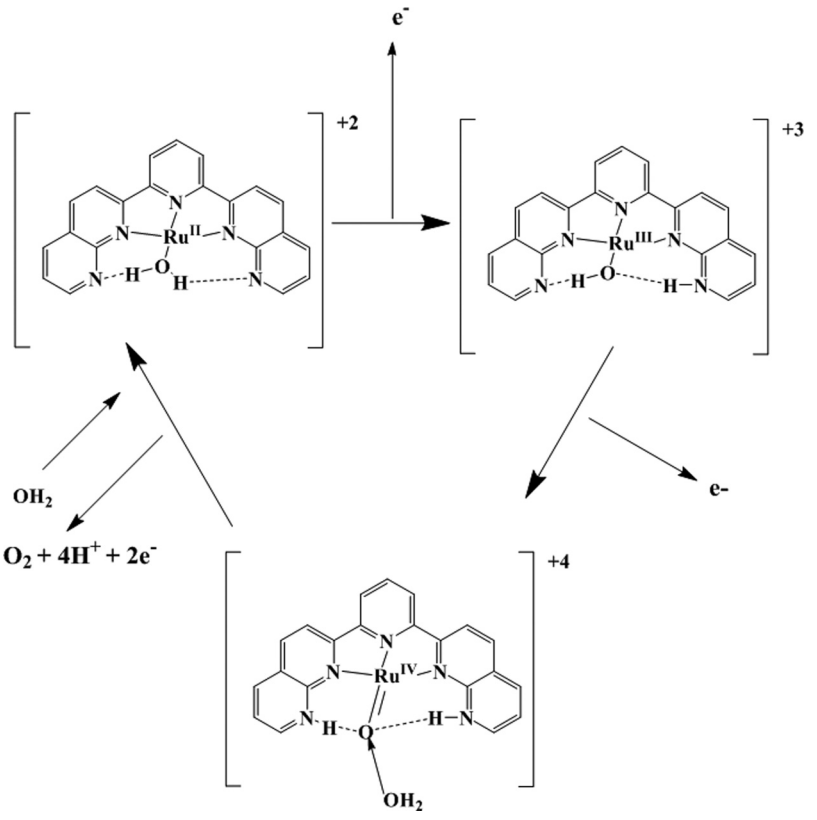

Scheme 2. Proposal mechanism for oxygen evolution.

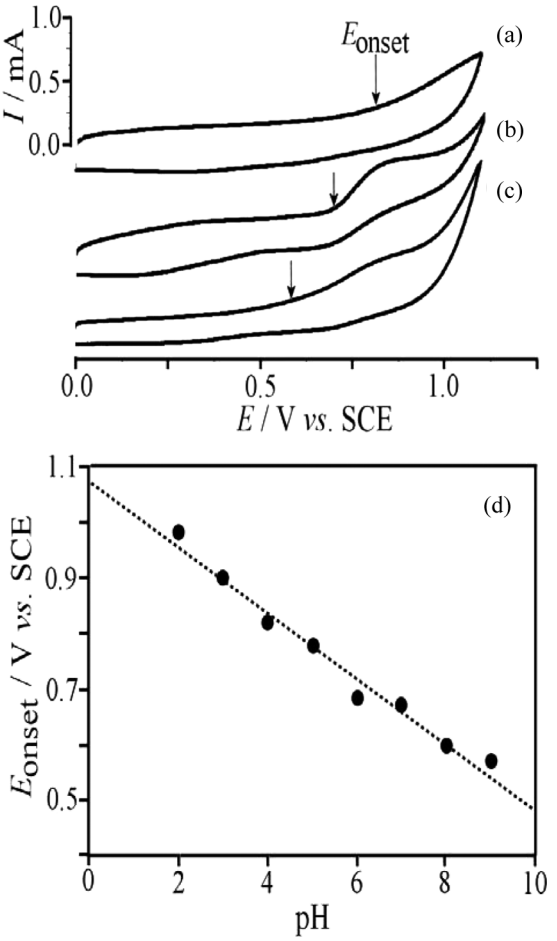

Figure 7. Cyclic voltammograms (scan rate $0.1\,V\,s^{-1}$) obtained for a complex modified basal plane pyrolytic graphite electrode at 40°C immersed in aqueous 0.1 M phosphate buffer at (a) pH 5, (b) pH 7, (c) pH 9, and (d) Plot of the approximate onset potential for the anodic current response P1 vs. the pH.

hydroxide ligand) and rapid follow-up processes would then lead ultimately to the formation of oxygen (Scheme 2). Phosphate in contrast to fluoride appears to affect the activity of the complex catalyst.

Solid State Electrochemical Characterization of The Complex in Aqueous NH_4NO_3 Electrolyte Media

Cyclic voltammograms (T = 35°C) obtained for the complex modified basal plane pyrolytic graphite electrode for different scan rates (i) 10, (ii) 50, and (iii) $100\,mV\,s^{-1}$ immersed in aqueous 10 g/l ammonium nitrate solution are shown in Fig. 8. The ammonium nitrate environment and the temperature were chosen to mimic the conditions during the Ce(IV) driven reaction. Initially, a clean graphite electrode was immersed into a solution of Ce(IV) nitrate, and the equilibrium

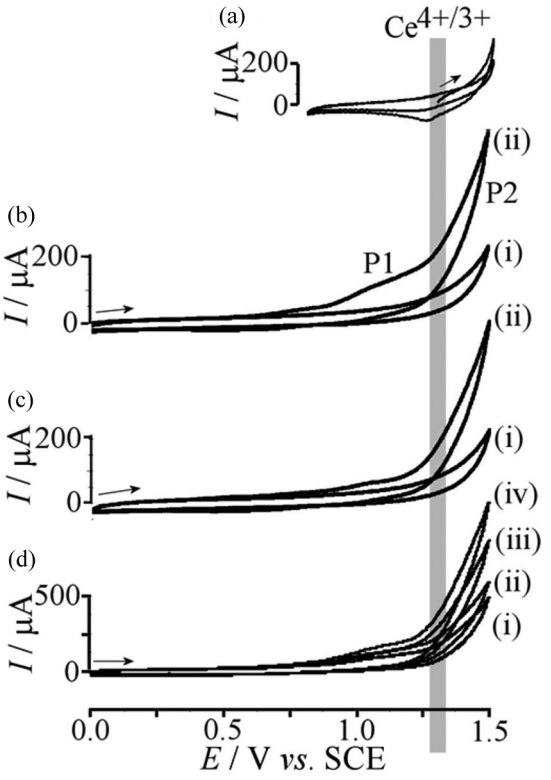

Figure 8. (a) Cyclic voltammograms (scan rate 50 mV s^{-1}, two cycles shown, T = 35°C) for the oxidation and reduction of a solution of 10 g dm^{-3} $(NH_4)_2Ce(NO_3)_6$ at a 4.9 mm diameter basal plane pyrolytic graphite electrode. The grey bar is indicating the initial equilibrium potential at 1.28 V vs. SCE. (b) Cyclic voltammograms (scan rate 50 mV s^{-1}, T = 35°C, first potential cycle) obtained at (i) a bare basal plane pyrolytic graphite electrode and (ii) a complex modified basal plane pyrolytic graphite electrode (4.9 mm diameter) immersed in aqueous 10 g dm^{-3} ammonium nitrate solution. (b) Second potential cycle. (d) Cyclic voltammograms (scan rate 50 mV s^{-1}, T = 35°C, first potential cycle) obtained for a complex modified basal plane pyrolytic graphite electrode immersed in aqueous 10 g dm^{-3} ammonium nitrate solution at (i) T = 25, (ii) 35, (iii) 45, and (iv) T = 55°C.

potential, 1.28 V vs. SCE, was noted (see Fig. 8a). Cycling the potential within a small range of this potential (see the grey zone in Fig. 8) shows weak responses associated with the Ce(IV/III) redox system in Fig. 8.

Conclusion

In this study a novel linear coordination polymer catalyst is synthesized and characterized. In the presence of $(NH_4)_2[Ce(NO_3)_6]$, the polymeric catalyst is found to react with water and to efficiently and continuously liberate molecular oxygen (O_2). In electrochemical experiments, this catalytic process was confirmed, the activation energy for this process was estimated, and the potential dependence of the catalytic process was revealed.

Acknowledgment

This work was supported by the Dorna Institute of Science and National Elite Foundation. Help with conducting and interpreting solid state electrochemical measurements by L. Rassaei and F. Marken (University of Bath, UK) is gratefully acknowledged.

References

[1] Yano, J., Kern, J., Sauer, K., Latimer, M. J., Pushkar, Y., Biesiadka, J., Loll, B., Saenger, W., Messinger, J., Zouni, A., & Yachandra, V. K. (2006). *Science*, *314*, 821–825.
[2] Collings, A. F., & Critchley, C. (2005). *Artificial Photosynthesis from Basic Biology to Industrial Application*, Wiley-VCH.
[3] (a) Cady, C. W., Crabtree, R. H., & Brudvig, G. W. (2008). *Coord. Chem. Rev.*, *252*, 444–455. (b) Rüttinger, W., & Dismukes, G. C. (1997). *Chem. Rev.*, *97*, 1–24. (c) Limburg, J., Vrettos, J. S., Liable-Sands, L. M., Rheingold, A. L., Crabtree, R. H., & Brudvig, G. W. (1999). *Science*, *283*, 524–527. (d) Naruta, Y., Sasayama, M. A., & Sasaki, T. (1994). *Angew. Chem. Int. Ed.*, *33*, 1839–1841. (e) Shimazaki, Y., Nagano, T., Takesue, H., Ye, B. H., Tani, F., & Naruta, Y. (2004). *Angew. Chem. Int. Ed.*, *43*, 98–100. (f) Yagi, M., & Kaneko, M. (2001). Chem. Rev., *101*, 21–35. (g) Pulsen, A. K., Rompel, A., & McKenzie, C. J. (2005). *Angew. Chem. Int. Ed.*, *44*, 6916–6920.
[4] Hurst, J. K. (2005). *Coord. Chem. Rev.*, *249*, 313–328.
[5] Sens, C., Romero, M., Rodŕıguez, M., Llobet, A., Parella, T., & Benet-Buchholz, J. (2004). *J. Am. Chem. Soc.*, *126*, 7798–7799.
[6] (a) Zong, R., & Thummel, R. P. (2005). *J. Am. Chem. Soc.*, *126*, 7798–7799. (b) Deng, Z., Tseng, H., Zong, R., Wang, D., & Thummel, R. P. (2008). *Inorg. Chem.*, *47*, 1835–1848.
[7] Rodriguez, M., Romero, I., Sens, C., & Llobet, A. (2006). *J. Mol. Catal.*, *251*, 215–220.
[8] Gajardo, J., Araya, J. C., Moya, S. A., Pardey, A. J., Guerchais, V., Le Bozec, H., & Aguirre, P. (2006). *Appl. Organometal. Chem.*, *20*, 272–276.
[9] Nakamoto, K. (1986). *Infrared and Raman Spectra of Inorganic and Coordination Compounds*. Fourth edition, A Wiley- Interscience Publication.
[10] Juris, A., Balzani, V., Barigelletti, F., Campagna, S., Belser, P., & Zelewisky, A. V. (1988). *Coord. Chem. Rev.*, *84*, 85–277.
[11] Mallick, P. K., Danzer, G. D., Strommen, D. P., & Kincaid, J. R. (1988). *J. Phys. Chem.*, *92*, 5628–5634.
[12] Strommen, D. P., Mallick, P. K., Danzer, G. D., Lumpkin, R. S., & Kincaid, J. R. (1990). *J. Phys. Chem.*, *94*, 1357–1366.
[13] McEvoy, J. P., & Brudvig, G. W. (2004). *Phys. Chem. Chem. Phys.*, *6*, 4754–4763.
[14] Najafpour, M. M. (2006). *Plant Biosystems*, *140*(2), 163–170.
[15] Bond, A. M. (2002). *Broadening Electrochemical Horizons*, Oxford University Press, Oxford.
[16] Marken, F., Cromie, S., & McKee, V. (2003). *J. Solid State Electrochem.*, *7*, 141–147.
[17] Bond, A. M., Cooper, J. B., Marken, F., & Way, D. M. (1995). *J. Electroanal. Chem.*, *396*, 407–418.